View metadata, citation and similar papers at core.ac.uk

brought to you by CORE

provided by IntechOpen

We are IntechOpen, the world's leading publisher of Open Access books Built by scientists, for scientists

4,800
Open access books available

122,000
International authors and editors

135M
Downloads

Our authors are among the

154
Countries delivered to

TOP 1%
most cited scientists

12.2%
Contributors from top 500 universities

CLARIVATE ANALYTICS BOOK CITATION INDEX INDEXED

WEB OF SCIENCE™

Selection of our books indexed in the Book Citation Index in Web of Science™ Core Collection (BKCI)

Interested in publishing with us?
Contact book.department@intechopen.com

Numbers displayed above are based on latest data collected.
For more information visit www.intechopen.com

14

Finite- and Quantum-size Effects of Bismuth Nanowires

Thomas W. Cornelius[1] and M. Eugenia Toimil-Molares[2]
[1]*European Synchrotron Radiation Facility (ESRF), B.P. 220, 38043 Grenoble Cedex*
[2]*GSI Helmholtz Institute for Heavy Ion Research GmbH, Planckstr. 1, 64291 Darmstadt*
[1]*France*
[2]*Germany*

1. Introduction

During the last decades, the miniaturization of electronic devices has strongly influenced the technological evolution. For instance, Moore's law states that roughly every 18 months the number of transistors per microchip doubles. This law has been valid remarkably well in the last 40 years and it is expected to hold for some more years to come. This process requires an ongoing reduction of feature sizes, and assumes that the components of a microchip can be scaled down arbitrarily without changes in their performance. However, conventional transport theories will fail on such small feature sizes. When the size is comparable to the mean free path l_e of the conduction electrons, the mesoscopic transport regime is entered leading to so-called finite-size (FSE) or classical-size effects. These effects include additional electron scattering processes both at the surface of the structure and at inner grain boundaries. When the structure size even reaches the Fermi-wavelength λ_F and, hence, the electronic wave function becomes confined, quantum-size effects (QSE) are expected to occur which involve a change of the density of states and, thus, affect the transport properties as well as the optical properties.

1.1 Bismuth

In order to study these confinement effects, bismuth is an ideal material because of its unique electronic properties. The electrons possess a large mean free path being in the range of 100 to 250 nm at room temperature that increases to the millimeter range at 4 K (Cronin et al., 2002). Further, they exhibit a long Fermi wavelength of 40 to 70 nm (Garcia et al., 1972; Duggal & Rup, 1969) which is more than one order of magnitude larger than in typical metals. Since both intrinsic length scales (l_e and λ_F) are large, finite-size as well as quantum-size effects can be investigated in comparatively large specimen. Furthermore, Bi is a semimetal with a very small indirect band overlap resulting in a low charge carrier density n compared with conventional metals (3×10^{18} cm^{-3} at 300 K, 3×10^{17} cm^{-3} at 4 K). The electron effective mass m^* in bismuth amounts to (0.001 – 0.26) m_e depending on the crystalline orientation with m_e being the free electron mass (Lin et al., 2000). This very small m^* facilitates the observation of QSE.

The current study of the transport properties of bismuth and bismuth compound nanowires is also partly motivated by theoretical studies, that predicted substantial enhancements of

Source: Nanowires, Book edited by: Paola Prete,
ISBN 978-953-7619-79-4, pp. 414, March 2010, INTECH, Croatia, downloaded from SCIYO.COM

the thermoelectrical figure of merit zT for low-dimensional materials (Lin et al., 2000). While in bulk materials the parabolic density of states $D(E)$ means that the electron density around the Fermi level is small, in one-dimensional structures such as nanowires the spikes in the $D(E)$ suggest that the thermal power factor $S^2\sigma$ can be intentionally increased in a controlled manner. In addition, thermal conductivity κ can be significantly reduced by phonon scattering at wire boundaries. Thus, a figure of merit zT = 6 at 77 K has been predicted for n-doped Bi nanowires with diameter 5 nm oriented along the trigonal axis (Lin et al., 2000). This efficiency approaches that of conventional vapor-compression unit and, thus, experimental evidence of such a zT enhancement would have a large impact on the thermoelectrics industry.

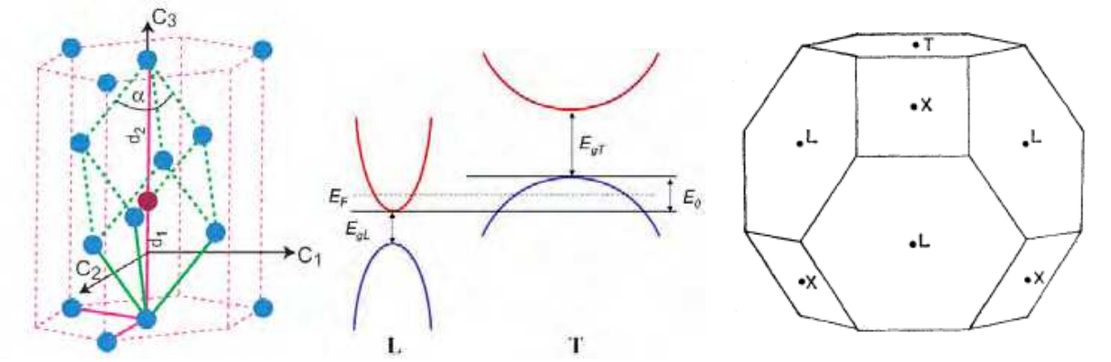

Fig. 1. a) Schematic of the rhombohedral lattice structure (dashed bold lines) of bismuth belonging to space group $R\bar{3}m$ together with the hexagonal unit cell (dashed thin lines) (Hofmann, 2005). The solid bold and thin lines are the vectors spanning the rhombohedral and hexagonal lattice, respectively. C_1, C_2, and C_3 are the bisectrix, binary, and trigonal axes. Schematics of b) the band structure and c) the Brillouin zone of bismuth.

Bismuth crystallizes in a rhombohedral lattice structure which belongs to the $R\bar{3}m$ space group with two atoms per unit cell. Alternatively, the structure can be described as hexagonal with six atoms per unit cell. The relation between these different unit cells is shown in Fig. 1(a) (Hofmann, 2005). The dashed bold and thin lines indicate the rhombohedral and hexagonal unit cell, respectively. Directions in the bismuth crystal are specified with respect to three mutually perpendicular directions which are marked by C_1, C_2, and C_3; C_2 – one of the three axes of twofold symmetry (binary direction), C_3 – the axes of threefold symmetry (trigonal direction), C_1 – an axis perpendicular to C_2 and C_3 forming a right-hand triad in the order 1-2-3 (bisectrix direction). The trigonal direction of the rhombohedral structure is the c-axis of the hexagonal lattice. The rhombohedral angle α = 57.23 ° is slightly distorted from its value of 60 ° in a perfect fcc lattice. This distortion leads to highly anisotropic Fermi surface and, thus, is largely responsible for bismuth's unique electronic properties. Due to the Fermi surface anisotropy all transport properties (electrical and thermal conductivities) and the effective masses of charge carriers depend on the crystalline orientation. Both thermal and electrical conductivities of bulk Bi are small compared to metals. The specific electrical resistivity amounts to about 135 and 110 μΩ cm at 300 K parallel and normal to the trigonal axis, respectively. At room temperature the thermal conductivity is about 10 and 6 W m^{-1} K^{-1} parallel and perpendicular to the trigonal direction, respectively (Gallo, 1962).

The band structure of bismuth is schematically depicted in Fig. 1(b). The electrons and holes are located at the L- and at the T-point of the Brillouin zone, respectively (Fig. 1(c)). A small indirect overlap E_0 is present between the valence band at the T-point and the conduction band at the L-point making Bi to a semimetal. Both at the L-point and at the T-point a direct band gap exists. The size of the gap at the L-point amounts to E_{gL} ~ 15 meV and ~ 36 meV at 0 and 300 K, respectively (Black et al., 2003). In contrast, the size of the gap at the T-point is rather unknown. In literature, values ranging from 50 to 400 meV can be found for room temperature (Bate & Einspruch, 1967; Isaacson & Williams, 1969; Omaggio et al., 1993). The Fermi energy E_F, whose value is defined with respect to the lower edge of the L-point conduction band, amounts to 26 and 56 meV at 0 and 300 K, respectively (Gallo et al., 1962). In the following sections the effect of low-dimensionality on the electronic properties will be described briefly.

1.2 Finite-size effects

Finite-size effects involve additional electron scattering from the wire surface as well as from grain boundaries within the wire leading to an increase of the specific electrical resistivity. Mayadas and Shatzkes developed a model for the influence of the electron scattering from grain boundaries on the electrical resistivity which depends on the mean grain size D, the mean free path l_e, and the reflexion coefficient R of the boundaries (Mayadas & Shatzkes, 1970).

$$\frac{\rho_0}{\rho_g} = 3\left[\frac{1}{3} - \frac{1}{2}\alpha + \alpha^2 - \alpha^3 \ln\left(1 + \frac{1}{\alpha}\right)\right] \text{ with } \alpha = \frac{l_e}{D}\frac{\mathscr{R}}{1-\mathscr{R}} \tag{1}$$

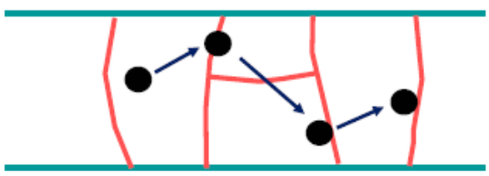

Fig. 2. Schematic of electron scattering from grain boundaries.

The influence of electron scattering at surfaces on the electrical transport properties was studied theoretically already in the first half of the last century. In the 1930's K. Fuchs developed a model to treat the electron scattering from the surface of thin films (Fuchs, 1938). This theory was extended to square shaped and cylindrical wires by MacDonald and Sarginson (MacDonald & Sarginson, 1950) and R.B. Dingle (Dingle, 1950), respectively. According to these theories the contribution of the electron scattering from the surface to the electrical resistivity depends on two parameters: (i) The specularity ε of the scattering processes with $0 < \varepsilon < 1$ and (ii) the ratio k of film thickness, respectively, wire diameter d and electron mean free path ($k = d/l_e$). The equations (2a) and (2b) are approximations for completely diffuse scattering ($\varepsilon = 0$) from the surface for cylindrical wires with diameters much smaller ($k << 1$) and much larger ($k >> 1$) than the electron mean free path [4], respectively. Expressions (2c) and (2d) are the analogical approximations for partly diffuse scattering processes ($\varepsilon = 0.5$).

$$\frac{\sigma}{\sigma_0} = 1 - \frac{3}{4k} + \frac{3}{8k^3} \cdots \tag{2a}$$

$$\frac{\sigma}{\sigma_0} = k - \frac{3k^2}{8}\left(\ln\frac{1}{k} + 1.059\right) - \frac{2k^3}{15} \tag{2b}$$

$$\frac{\sigma}{\sigma_0} = 1 - \frac{0.375}{k} + \frac{0.109}{k^3} \cdots \tag{2c}$$

$$\frac{\sigma}{\sigma_0} = 3k - 11.22k^2\left(\log\frac{1}{k} - 0.245\right) - 9.74k^3 \tag{2d}$$

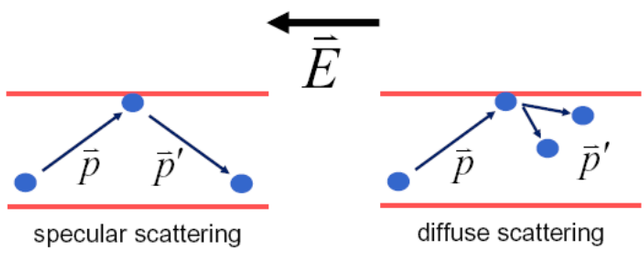

Fig. 3. Schematic of specular and diffuse scattering of electrons from the wire surface. E is the applied electrical field.

Note that the models are simplified in so far that they assume materials having a spherical Fermi surface and that they do not take into account the angle of incidence of the charge carriers on the surface. J.E. Parrott improved Fuchs' theory to materials having spheroidal and ellipsoidal Fermi surfaces and by introducing a critical wave vector K_0 which depends on the angle of incidence θ of the electrons on the surface (Parrott, 1965). By this approach the reflection coefficient becomes a function of the wave vector and, thus, of θ. When the wave vector is less than K_0 the reflection coefficient is $\varepsilon = 1$ and $\varepsilon = 0$ for $K > K_0$, i.e., the scattering from the surface becomes specular for $\theta < \theta_0$ while it becomes abruptly completely diffuse for $\theta > \theta_0$. Barati and Sadeghi extended this model to nanowires of materials with non-spherical Fermi surfaces, in particular, for bismuth nanowires (BS model) (Barati & Sadeghi, 2001). For bismuth nanowires oriented normal to the trigonal axis, the conductivity can be written as

$$\sigma = \frac{\sigma_{bulk} a_1}{\sqrt{\det a}}\left[1 - \frac{6}{k}\int_{\mu_0}^{1} \exp\left(-\frac{k}{2\mu}\right)\left[1 - \exp\left(-\frac{k}{2\mu}\right)\right]\mu^2\sqrt{1-\mu^2}\,d\mu\right] \tag{3}$$

where $\mu = \sin\theta$, $k = r/l_e$, σ_{bulk} is the electrical conductivity of bulk bismuth, and α is the reciprocal mass tensor.

1.3 Quantum-size effects

As the system size decreases and approaches nanometer length scales, it is possible to cause dramatic variations in the density of electronic states $D(E)$ which is schematically depicted

for different dimensionalities in Fig. 3. This dramatic change is caused by the spatial confinement of the electronic wavefunction. While for 3-D materials $D(E) \sim \sqrt{E}$, in quasi-one-dimensional structures – such as nanowires – it exhibits a spike-like shape arising from discrete energy levels due to a splitting of the energy bands into subbands. This gives rise to manipulate the electronic properties of the material and to utilize the electronic transport properties of various quasi-1D materials systems for a wide range of practical devices. For instance, according to Sandormirskii (Sandormirskii, 1967) and Farhangfar (Farhangfar, 2006), semimetallic thin films and rectangular nanowires show oscillating transport properties caused by the subband splitting.

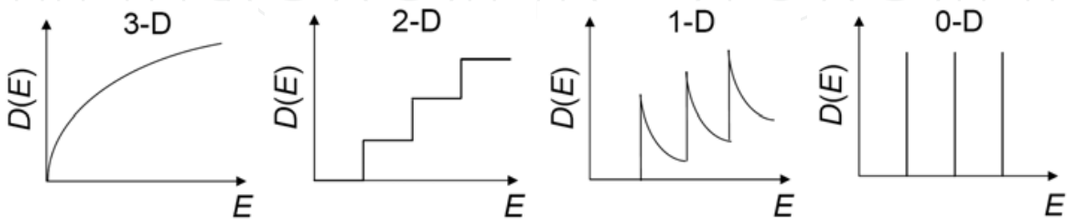

Fig. 4. Density of electronic states $D(E)$ for different dimensionalities

With decreasing structure size the energy separation between the subbands increases and, consequently, the edges of the energy bands shift away from each other. In the simplest case, a nanowire can be modelled as a two-dimensional infinitely deep potential well leading to the following equation for the energy shift that the band edges experience with N being the number of the subband and d the wire diameter.

$$\Delta E \approx \frac{N^2 \hbar^2 \pi^2}{m^* d^2} \tag{4}$$

Since the electron effective mass is comparatively small in bismuth, QSEs are strongly pronounced in this material. Note that the valence and the conduction band at the L-point are strongly coupled leading to an increasing electron effective mass with increasing band gap. The dispersion relation for the L-point bands is described by the Lax two-band model (Lax et al., 1960) (see equation (5)). For interband transitions, transitions between the n-th valence subband to the n-th conduction subband are allowed, where $|\langle v|p|c\rangle|$ is the coupling between the valence subband v and conduction subband c, and m_e is the free electron mass. At the band edge ($k = 0$), the momentum matrix element for the different subband states is the same, i.e., as the band gap enlarges, $|\langle v|p|c\rangle|$ remains constant, and the effective mass increases (Black et al., 2002).

$$\frac{1}{m^*} = \frac{1}{m_e} + \frac{2}{m_e^2} \frac{\left|\langle v|p|c\rangle\right|^2}{E_g} - \frac{12\hbar^2 k^2 \left|\langle v|p|c\rangle\right|^4}{E_g^3 m^2} \tag{5}$$

Owing to the spike-like $D(E)$ for 1D nanowires, the kinetic properties of the system will oscillate as a function of d, as long as the carrier gas is degenerate. These oscillations are connected with abrupt changes of the density of states on the Fermi surface as one subband after another passes E_F. According to Sandormirskiĭ (Sandormirskiĭ, 1967) and Farhangfar (Farhangfar, 2006), the periodicity for films and rectangular nanowires is given by the

critical thickness and width, respectively. Assuming that the Fermi level does not shift with the wire diameter, and according to equation (4), the critical diameter d_c is approximately given by

$$d_c \approx \frac{N\hbar\pi}{\sqrt{\Delta E\, m^*}} = \frac{Nh}{\sqrt{4E_F m^*}} \tag{6}$$

Figure 5 displays the computed band-edge energies as a function of the nanowire diameter with respect to the energy of the band edge of the L-point conduction band in bulk Bi. For calculations, the values E_{gL} = 36 meV, E_0 = 98 meV, E_F = 56 meV, and E_{gT} = 200 meV are used. In Fig. 5(a), the electron effective mass is assumed to be constant, namely m^* = 0.002 m_e, whereas in 5(b) the Lax two-band model has been taken into account. The strong coupling of electrons and holes at the L-point leads to a smaller energy shift of the band edges at the L-point for a given wire diameter. In addition to the shift of the band edges, the Fermi energy increases with diminishing wire diameter. The rise of E_F occurs in order to obtain charge neutrality, i.e., for achieving the same number of electrons and holes. At a critical wire diameter d_c the lowest subband of the conduction and the highest subband of the valence band do not overlap anymore. Thus, bismuth nanowires undergo a transition from a semimetal to a semiconductor at d_c of about 35 nm and 70 nm for calculations with and without incorporating the dependence of m^* on the band gap, respectively. Note that d_c is a function of the crystalline orientation due to the highly anistropic Fermi surfaces, resulting in a dependence of the electron effective mass on the crystalline direction. Lin et al. predicted the semimetal-semiconductor-transition to take place at 77 K for nanowires of d_c = 45, 44, 33 and 20 nm oriented along $\left[10\bar{1}1\right]$, bisectrix, trigonal and binary axis, respectively (Lin et al., 2000).

Note that in order to observe QSEs two preconditions have to be satisfied: (i) The relaxation time τ must be sufficiently long, i.e., $\tau > \hbar/(E_{n+1} - E_n)$ with $(E_{n+1} - E_n)$ being the energy separation between two subbands at the Fermi level. (ii) The thermal broadening of the levels must be small compared to the subband splitting. In order to fulfil the first requirement, the specimens must consist of grains much larger than l_e, and should possess only a small number of defects. In order to meet the second precondition, the subband splitting at the Fermi level must exceed the thermal broadening (e.g. 25 meV which corresponds to kT at 300 K). A number of studies exist reporting QSE at room temperature for Bi thin films with thicknesses > 100 nm (Duggal & Rup, 1969; Rogacheva et al., 2003). Since nanowires confine the electronic wavefunction in two instead of only one dimension like in thin films, quantum size effects are expected to occur at diameters larger than the reported film thicknesses and, hence, QSE can be investigated in few hundred nanometer thick wires.

1.4 Wear-out failure

An important aspect for components based on nanowires or carbon nanotubes (CNTs) is the maximal current density such quasi one-dimensional structures are able to carry. Bulk metals fail because of Joule heating at current densities of 10^3 to 10^4 A/cm^2 (Ho & Kwok, 1989) while CNTs can carry 10^9 A/cm^2 (Dai et al., 1996). In the case of bulk bismuth, the specific electrical conductivity and the thermal conductivity are more than 50 times smaller than for metals and the melting temperature amounts only to T_m = 544 K. Consequently, Bi

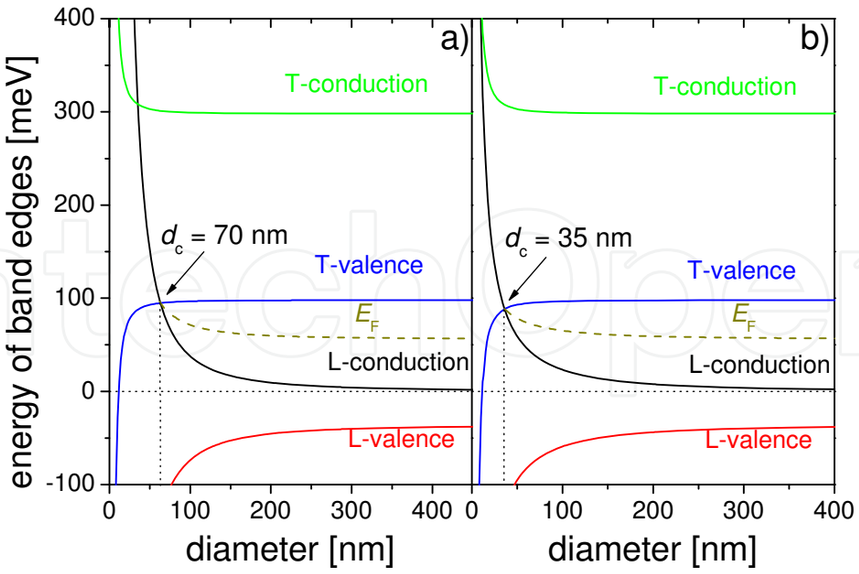

Fig. 5. Energy of the band edges as a function of the wire diameter: a) $m^* = 0.002\ m_e$ = const, b) employing the Lax two-band model with $m^* = 0.002\ m_e$.

is expected to fail at one to two orders of magnitude lower current densities. High critical current densities of the order of 10^6 A/cm^2 can be observed in microstructured metal lines, which serve as interconnects in microelectronic circuits. These metal lines are fabricated by photolithographic patterning on silicon wafers. Because of the intimate thermal contact of the film to the substrate with high thermal conductivity (150 W m^{-1} K^{-1} for silicon), the Joule heat can be dissipated immediately to the substrate and, therefore, higher current densities compared to suspended metal wires can be observed. In addition to Joule heat dissipation, another effect was identified in microelectronics as a potential wear-out failure for devices that employ metal film conductors, namely electromigration (Black et al., 1969). Electromigration is a mechanism for transport of matter by high electric current densities: when a metal ion is thermally activated and is at its saddle point, i.e., it is lifted out of its potential well and is essentially released from the metal lattice, two opposing forces act in an electrically conducting single-band metal: (i) the electric field applied induces a force on the activated positive ion in the direction opposite to the flow of the conduction electrons. (ii) The rate of momentum exchange between the electrons colliding with the ions exerts a force on the metal ions in the direction of the electron flow. Because of the shielding effect of the electrons, the force on the ions due to the electric field is quite small and, hence, the predominant force is that of the "electron wind". This causes dramatic failures in interconnects and it has been shown that is material, geometry and size-dependent.

2. Nanowire synthesis and structural characterization

Because of the low melting point of bismuth the synthesis of Bi nanowires is rather difficult. Most of the existing high-temperature approaches like laser ablation, plasma-arc or chemical vapour deposition are not appropriate for their fabrication. However, several different techniques exist for Bi nanowire preparation including solvothermal synthesis (Gao et al., 2003), the Taylor process (Glocker & Skove, 1977), electron beam writing techniques (Chiu &

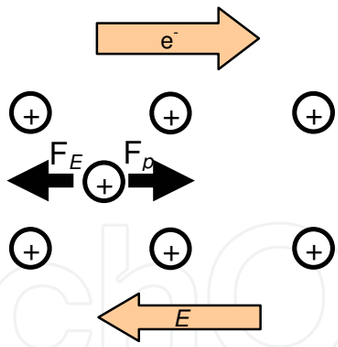

Fig. 6. Schematic of forces acting on a thermally activated ion at its saddle point in a conductor.

Shih, 2004), and the template method (Cornelius et al., 2005; Huber et al., 2003; Wang et al., 2001; Yin et al., 2001; Zhang et al., 1998). Solvothermal synthesis provides nanowires of good crystalline quality with diameters down to 40 nm and with lengths of several μm. By using the Taylor process, single-crystalline Bi nanowires were created by filling a glass tube with metal and, subsequently, drawn into a thin capillary. The drawback of this method is the fact that the temperature must exceed the softening point of glass and, as a consequence, the wires may be contaminated. Electron beam lithography enables the creation and electrical contacting of rectangular bismuth wires with lengths of several tens of micrometers, thickness 50 nm and width in the range of 70 – 200 nm. However, the wire crystallinity that strongly influences all transport properties cannot be controlled by this approach. In the case of polycrystalline materials electron scattering at the grain boundaries leads to higher resistivity values than for single-crystalline ones. Furthermore, grain boundaries are locations at which electromigration-driven failure predominantly occurs. Moreover, in the case of bismuth, due to its highly anisotropic Fermi surface, the properties of the material are highly dependent on the crystalline orientation. The most common technique is the template method which is a very general approach used to prepare arrays of nanomaterials. The most commonly used nanoporous templates are track-etched polycarbonate membranes (Martin, 1994; Toimil Molares et al., 2001; Cornelius et al., 2005; Karim et al., 2006) and porous anodic aluminum oxide (AAO) membranes (Masuda & Nishio, 2006; Heremans et al., 2000; Huber et al., 2003; Zhang et al., 1998). Common to all these templates is the fact that the pores are perpendicular to the surface of the membrane. Bismuth was synthesized in the pores by several techniques, most commonly by high-pressure injection (Huber et al., 2003; Zhang et al., 1998) and the electrochemical deposition of bismuth into the channels (Wang et al., 2001; Yin et al., 2001; Cornelius et al., 2005).

2.1 Template fabrication

- Anodic alumina oxide (AAO) templates (Masuda & Nishio, 2006)

Porous anodic aluminum oxide templates are fabricated by anodizing aluminum sheets in an oxalic acid solution. During this process, cylindrical pores with diameter 7 – 200 nm are self-assembled into a hexagonal array. The pore diameter and the distance between the pores are controlled systematically by varying the anodization voltage and the electrolyte used. The thickness of the alumina template determines the wire length, and can be controlled by the anodization time. By this method, templates containing a high density of pores of up to 10^{10} pores per cm^2 can be prepared. Thus, leading to densely packed nanowire arrays.

- Ion track-etched membranes

To fabricate ion track-etched membranes, polycarbonate foils tens of micrometers thick are irradiated with swift heavy ions. The charged particles modify the material along their trajectory creating cylindrical volumina – so-called ion tracks – which behave chemically different to the non-irradiated foil. Tracks in polycarbonate are selectively dissolved in aqueous sodium hydroxide. Prior to the chemical etching the foils are treated by UV light for sensitizing them to the leach. The pore density is given by the applied ion fluence and vary between 1 single pore per foil and 5 x 10^9 pores/cm^2. The pore diameter increases linearly with the etching time, and the etching rate depends on the etchant concentration and temperature.

Single nanochannel membranes are fabricated at the GSI Helmholtz Center for Heavy Ion Research GmbH, by single ion irradiation and chemical etching (Apel et al., 1999; Siwy et al., 2003; Cornelius et al., 2007). Single ion irradiation is performed by defocusing the ion beam so that ~ 10^4 ions/cm^2 reach the sample. A mask with a 100 micrometer aperture is placed in front of the sample, and a detector is placed behind the sample. As soon as an ion reaches the detector, a chopper deflects the ion beam. With this set up, single-ion irradiation or irradiation with a preset number of ions can be performed. For the etching of single-track membranes, the irradiated polymer foil is placed between two compartments of an electrolytical cell, using a 2M NaOH solution at 60 °C as etchant and a gold rod as electrodes is immersed on each side (Chtanko et al., 2004). During etching a potential is applied between the two electrodes and the current is recorded as a function of the etching time. After etching, the membrane is rinsed with distilled water. The effective pore diameter d_{eff} of a single nanopore is determined by conductivity measurement with 1 M KCl solution and two Ag/AgCl electrodes. By means of the following equation d_{eff} is calculated assuming an ideal cylinder

$$d_{eff} = \sqrt{\frac{4L}{\pi\kappa}\frac{I}{U}} \tag{7}$$

with L being the length of the pore, i.e., the membrane thickness, U is the applied voltage, κ is the conductivity of the 1 M KCl solution (κ = 10 S/m at 20 °C), and I is the recorded current.

Ion track-etched membranes can also be purchased e.g. from Whatman company. However, misalignment of the pores (tilted up to 34°) and cigar-like shapes of the commercial membrane pores have been reported (Schönenberger et al., 1997).

2.2 Nanowire growth and characterization

Bismuth nanowires have been grown in templates using different growth techniques, and few of them are shortly described in as following:

i. *Pressure injection*: Molten bismuth was pressed by high pressure into the pores of AAO membranes. Afterwards, the setup was cooled down leading to recrystallization of the molten material within the nanopores. Since the pressure needed for pushing the melt into the pores scales inverse with the pore diameter, this techique is limited to pores with a diameter of few ten nanometers (Huber et al., 2003; Zhang et al., 1998).
ii. *Vapor phase technique*: For this purpose, a heater containing bismuth and being covered by an AAO template is heated to temperatures of 400 to 500 °C. At this temperature

bismuth evaporates and penetrates the nanopores. Then, a slow cool-down phase is intiated. Since the top plate is cooler than the crucible, bismuth starts to condense at the top-side of the porous plate downwards. When the temperature has fallen below the melting temperature of Bi (271 °C) the process is finished. This method allowed the creation of nanowires with diameters down to 7 nm (Heremans et al., 2000).

iii. *Electrochemical deposition (Fig. 7)*: Electrochemical deposition of bismuth in nanopores has been reported using two different electrolytes based on $Bi(NO_3)_3$ (Wang et al., 2001) and $BiCl_3$ (Cornelius et al., 2005). One side of the template was coated by a conductive layer that served as cathode during the subsequent electrochemical deposition of bismuth inside the nanopores. In most cases, depositions were performed potentiostatically. Reverse pulse deposition at both low and high frequency have also been reported. For potentiostatic and low frequency reverse pulse depositions the wires fill the complete nanopore cross-section. In contrast, for high-frequency depositions the needles possess a smaller diameter than the pores and, thus are free-standing within the template (Li et al., 2005).

Fig. 7. Schematic of the electrochemical deposition template method: a) nanoporous membrane, b) deposition of a conductive layer on one side of the template, c) growth of the naowires inside the pores.

2.3 Nanowire crystallinity

The crystallinity of nanowires prepared in templates by the different synthesis methods has been investigated by several groups by X-ray diffraction (XRD) as well as transmission electron microscopy (TEM) including selected-area electron diffraction (SAED). As expected, crystallinity and preferred orientation reported for the bismuth nanowires differs depending on the fabrication technique. Single-crystalline Bi nanowires oriented along the [102] direction were prepared by a low-temperature solvothermal processn (Gao et al., 2003). Nanowires with diameters 40 and 95 nm created by high-pressure injection in alumina templates exhibited a <202> and <012> texture, respectively, indicating that the preferred crystalline orientation is a function of the wire diameter (Lin et al., 2000). Nanowires grown by the vapor technique possess a <202> texture as 40-nm diameter wires grown by pressure injection (Heremans et al., 2000). Bismuth nanowires fabricated by potentiostatic electrodeposition exhibited in all cases a single-crystalline <110> texture independently of the template and of the bath that was used (Cornelius et al., 2005; Wang et al., 2001). When using a bismuth chloride electrolyte, a pronounced increase of the <110> texture with decreasing overpotential and rising temperature. Fig. 8(a) displays the θ-2θ scan for an array of nanowires deposited at -17 mV and 60 °C revealing a very pronounced <110> texture. The single-crystallinity was proven by rocking curves around the <110> direction (Fig. 8(b)). In (Cornelius et al., 2005), the authors reported an increase in the texture with diminishing wire diameter. The preferred orientation of the crystals can be varied by applying reverse

pulses instead of a constant potential during the deposition process. As can be seen from the rocking curves around the <110> direction (inset of Fig. 8(b)) for short cathodic cycles t_c and high anodic potentials U_a, <100> textured wires were obtained. This preferential orientation becomes less pronounced for longer t_c and lower U_a while the <110> texture becomes stronger.

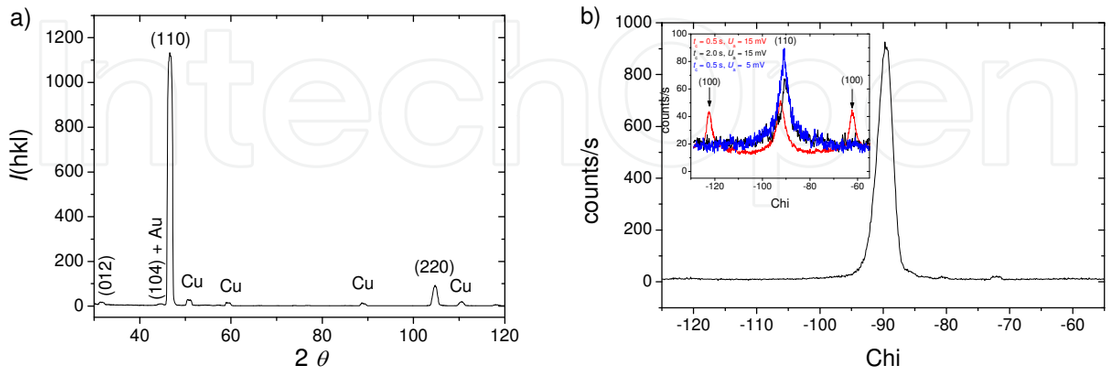

Fig. 8. a) θ-2θ scan and b) rocking curve for bismuth nanowire array deposited at -17 mV and 60 °C. The inset shows rocking curves for nanowires deposited applying reverse pulses.

For transmission electron microscopy studies, the template was removed and the wires were subsequently placed onto a TEM grid. Fig. 9(a) presents an overview of bismuth nanowires with diameter 80 nm grown potentiostatically at 60 °C and- 17 mV. In the image, the wires attach to the structures of the TEM grid exhibitng great flexiblility. Further, the micrograph demonstrates the smooth contour of the wires as well as the homogeneous diameter along the wire length. A high-resolution TEM (HRTEM) micrograph and a SAED pattern of a wire with diameter 30 nm are displayed in Fig. 9(b) and (c), respectively. The HRTEM image shows the atomic lattice of the wire demonstrating the single-crystalline character of the wire being supported by the SAED pattern which displays regular diffraction signals. Further, the diffraction pattern evidences that the wire is oriented along the <110> direction coinciding with the results obtained by XRD.

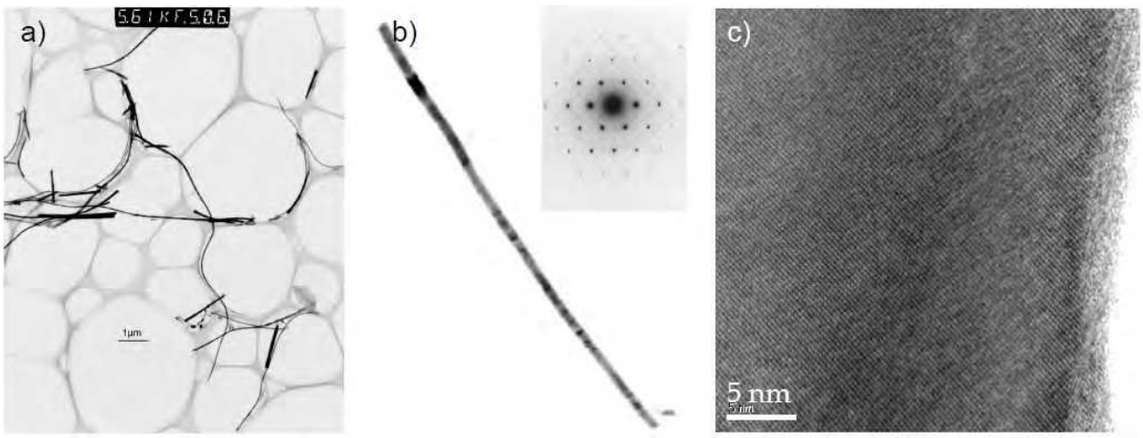

Fig. 9. a) TEM image of Bi nanowires with diameter 80 nm. b) TEM micrograph of Bi nanowire with diameter 50 nm and correspondent SAED pattern. c) High resolution TEM image of the same Bi nanowire.

Due to their high surface-to volume ratio of nanostructures, surfaces influence strongly the properties of nanowires. Alumina templates can be only removed with either strong acids or sodium hydroxide, and studies revealed that solvents used for dissolving the AAO template may attack and modify the wire surface. Thus, a comparatively thick oxide layer (~ 7nm) has been found on bismuth wire surfaces after dissolution of the template (Cronin et al., 2002). Polymer membranes are dissolved by organic solvents such a dimethylformamide (DMF, C_3H_7NO) and dichloromethane (CH_2Cl_2). Figures 10(a) and (b) display TEM images of two nanowires deposited in the same template, but from two different sample areas dissolved either in dichloromethane (Fig. 10(a)) or in dimethylformamide (Fig. 10(b)). In contrast to DMF, dichloromethane as solvent modifies the surface of the wires being marked by a bracket. The layer consists of a material that possesses a larger interlattice plane distance than bismuth. On top of this layer, an amorphous material is observed that contains most probably polymer residuals. Energy dispersive X-ray analysis (EDX) and the Fourier transform of the micrograph in Figure 10(c), reveal a modified surface layer consisting of bismuth oxychloride (BiOCl) piling up along the c-axis, i.e., normal to the wire axis, presumably developed during or after the dissolution of the template in dichloromethane (CH_2Cl_2).

For further processing such as lithographical contacting of single wires for electrical resistance measurements such surface layers must be avoided. Thus to avoid that large contact resistances hinder reliable measurements, a careful choice of the template solvent is required.

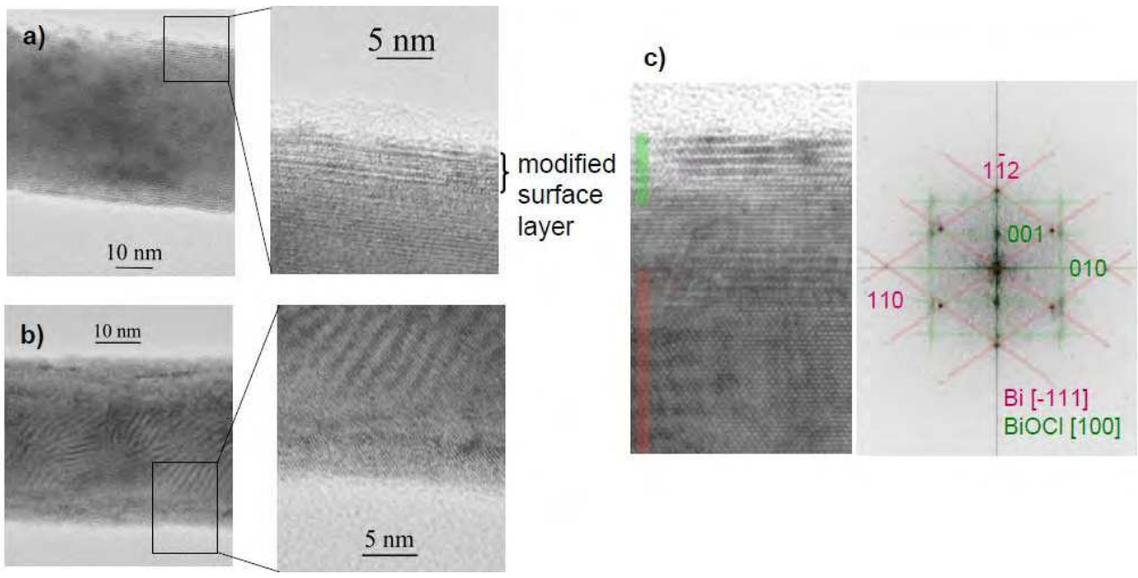

Fig. 10. High-resolution transmision electron micrographs. The templates were removed by a) dichloromethan (CH_2Cl_2) and b) dimethylformamide. c) HRTEM combined with SAED and EDX reveals that the surface layer consists of BiOCl.

3. Electrical transport properties

For investigating the electrical transport properties of low-dimensional systems, the electrical resistivity of bismuth nanowire arrays as well as of single wires were studied. In the case of arrays a pseudo-four-point contacting method was employed, i.e., the wires were

left embedded in the template (AAO or ITPC membrane) and on each side of the membrane two leads were fixed by a conductive glue (Fig. 11(a)). One lead on each side serves for measuring the potential drop and the other one for the electrical current. The contact resistance cannot be determined by this method but at least the resistance of the leads does not affect the measurement. Since the exact number of contacted nanowires is unknown, absolute values of the electrical resistivity cannot be determined in the case of arrays. To measure absolute values of the nanowire resistance, measurements at the single nanowire level are needed. Different approaches have been reported for contacting single wires.

As mentioned above, nanowire arrays were created in alumina templates by high-pressure injection of molten bismuth into the pores, the matrix being subsequently removed using an oxidizing acid. Since the wire surface was oxidized by this strong acid, the wires could not be reliably contacted by lithography (Cronin et al., 2002). Single wires with rectangular cross-section were prepared on a Si substrate by an electron beam writing technique. Bonding pads were formed on the oxide employing filament evaporation and optical lithography. Such wires were subsequently treated by reactive ion etching in order to reduce their dimensions. With this method, electrical transport measurements on the same wire with incremental reductions in diameter. However, this approach may affect the surface roughness of the wire and, hence, influence the transport characteristics (Farhangfar, 2007). Both experiments used a contacting approach as schematically depicted in Fig. 11(b).

Single bismuth nanowires were grown in single-pore ion track-etched polycarbonate membranes (Toimil Molares et al., 2004; Cornelius et al., 2006; Cornelius et al., 2008). After growth of the nanowire and the formation of a cap on top of it, this wire was left embedded in the template. Thus, the wires were protected against oxidiation and, in particular, not endangered by chemical reactions with a matrix solvent. In order to contact the embedded needles electrically an additional gold layer was sputtered on the cap grown on top of the wire and the complete sample was placed between two macroscopic copper plates (Fig. 11(c)).

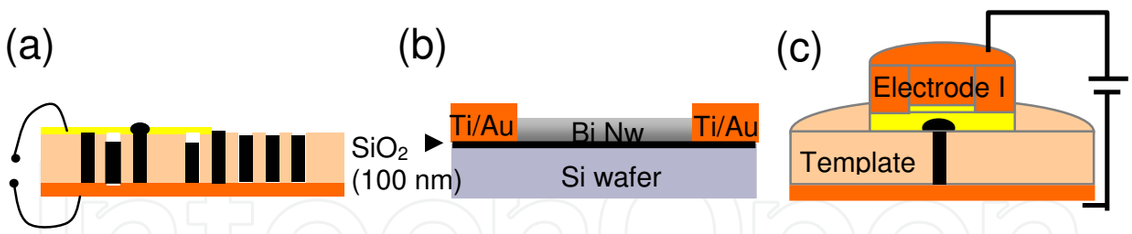

Fig. 11. Schematics of different methods for contacting single nanowires electrically: a) An undetermined number of wires in a multipore template. b) Single nanowire on a Si/SiO_2 substrate contacted by lithographic methods. c) Single nanowire electochemically grown in a single nanopore membrane and contacted by two macroscopic metallic layers.

3.1 Finite-size effects

Finite-size effects on the electrical transport properties of single bismuth nanowires were studied on wires grown electrochemically under different deposition conditions. By employing three different sets of deposition parameters (temperature and voltage), nanowires with diameters between 200 and 1000 nm with different average grain size D were successfully synthesized. The scanning electron micrographs (Fig. 12) of caps grown on top of the three types of wires show the variation of the mean grain size as a function of

deposition parameters. Each single nanowire was electrically contacted using the setup shown in Fig. 11(c). The specific electrical resistivity of wires with diameter > 150 nm was calculated from the *I-U* characteristics and is plotted as a function of the diameter in Fig. 12. The data evidence that nanowires deposited at lower *U* and higher *T*, i.e. with larger grain size (red circles) exhibited the lower resistivity values, while nanowires deposited at higher *U* and lower *T*, i.e. with the smallest grain size (green squares), exhibited the larger resistivity values. The specific resistivity amount to 850, 440, and 315 μΩ cm, i.e. 7.5, 3.8, and 2.8 times larger than the bulk resistivity (solid black line), for the three types of nanowires, increasing with decreasing mean grain size. This is in good qualitatively agreement with the MS model presented by Mayadas and Schatzkes (Mayadas & Shatzkes, 1970). It is remarkable that even for nanowires built up by large grains the specific electrical resistivity is about threefold the bulk value.

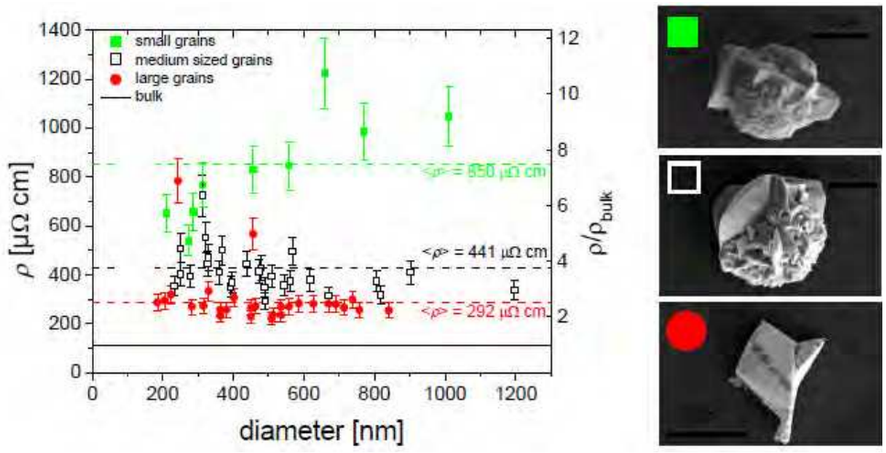

Fig. 12. Specific electrical resistivity of single Bi nanowires deposited under three different conditions leading to three different mean grain sizes. Scanning electron micrographs of nanowire caps representing the different grain size for the different types of wires.

Different groups reported measurements of the resistance of bismuth nanowires as a function of temperature, revealing different behaviours (Cornelius et al., 2006; Heremans et al., 2000; Liu et al., 1998; Zhang et al., 2000). For nanowire arrays prepared by high-pressure injection in alumina templates and for single wires electrochemically deposited in single-pore ion track-etched membranes with d > 200 nm a non-monotonic resistance versus temperature behaviour was reported. The resistance increased, passed a maximum, and declined when cooling down the wires from 300 to 10 K (Fig. 13(a)). The resistance maximum shifts to lower temperatures and the residual resistance becomes larger for increasing wire diameter. The same trend is observed for nanowire arrays (Kaiser et al., 2009) (Fig. 13(b)).

The non-monotonic behavior, when lowering the temperature, was attributed to the opposite contributions of decreasing charge carrier density n and increasing mobility μ to the electrical resistivity $\rho = ne\mu$. In bulk Bi, the gain in mobility surpasses the reduction of charge carrier density, leading to a monotonic decrease of resistivity with lowering T. In contrast, $l_e \sim \mu$ is limited in nanowires by both wire diameter and grain size, and thus the gain in mobility is limited due to finite-size effects (Fig. 14). These converse effects (decreasing number of phonons, increase and limitation of l_e, and decreasing n) lead to the

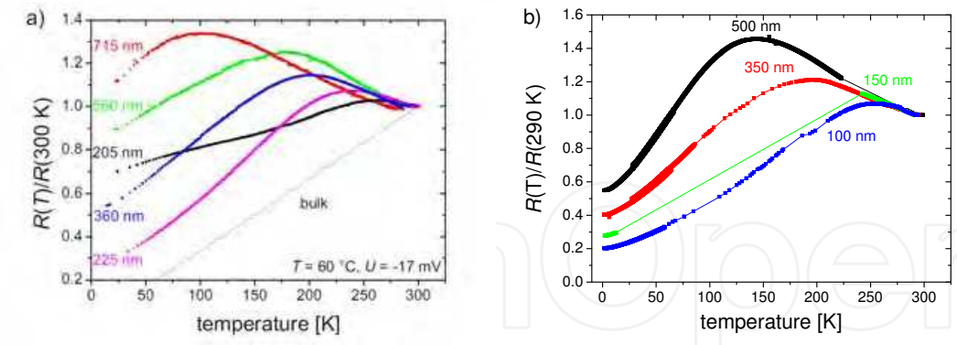

Fig. 13. Electrical resistance as a function of temperature for a) single Bi nanowires and b) nanowire arrays.

observed non-monotonic R vs T curve. In (Cornelius et al., 2006), the temperature dependence of the electron mobility for single Bi nanowires was calculated from the resistance data evidencing that μ saturates at few ten Kelvin. The saturation value was one to two orders of magnitude smaller than in bulk bismuth, and depended on both mean grain size and wire diameter. For wires of similar diameter, μ increases with growing mean grain size due to the decrease of electron scattering processes from grain boundaries when increasing D. For wires created under the same conditions, the smaller the wire diameter, the higher the mobility. This dependence can be explained either by the fact that thinner wires are formed by larger grains or that charge carrier density is affected by d.

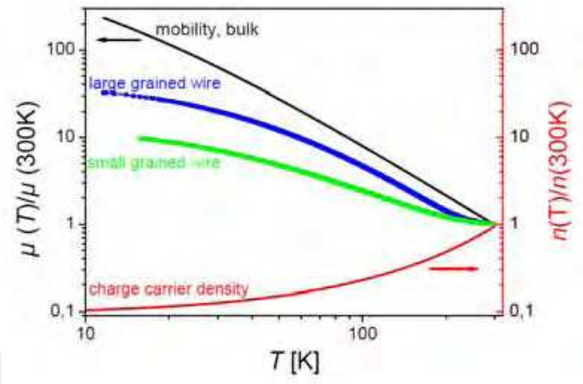

Fig. 14. Mobility of charge carriers in bulk bismuth and bismuth nanowires as well as the charge carrier density in Bi as a function of temperature.

In contrast to the non-monotonic $R(T)$ behaviour a monotonic increase of the resistance with decreasing temperature was reported for wires with diameters ranging from 200 nm to 2 µm prepared electrochemically in alumina templates (Liu et al., 1998). The authors attributed these observations to the fact that the wires possessed very small mean grain size, that in turn lead to a strong limitation of the carrier mobility. The same behaviour was found for wires with d < 50 nm created by the vapour-phase technique in alumina templates and for rectangular wires having a thickness of 50 nm and a width ranging from 75 to 200 nm created by the electron beam writing technique. This finding may be attributed either to the smallness of the grains like in the case before or to the fact that the wire width is close to the

predicted critical diameter for the semimetal-semicondcutor transition. Thus, the observation may also be explained by a semiconductor like behaviour.
Numerous works concentrated on the magnetoresistance (MR) of bismuth nanowire arrays. In (Liu et al., 1998) the authors reported a very large positive magnetoresistance of 300% at low temperatures and 70% at room temperature with a quasilinear field dependence. Moreover, MR measurements on Bi nanowire arrays at low temperatures revealed a steplike increase that was attributed to a transition from one-dimensional to three-dimensional localization (Heremans et al. 1998; Kaiser et al., 2009). In addition, a dependence of the low temperature resistance of individual single-crystal bismuth nanowires on the Aharonov-Bohm phase of the magnetic flux threading the wire was reported (Nikolaeva et al., 2008).
Recently, also superconductivity was reported for nano-granular bismuth nanowires that were prepared electrochemically (Tian et al., 2006). The critical temperatures T_c amount to 7.2 and 8.3 K which coincide with T_c values of the high-pressure phases Bi-III and Bi-V formed at 2.7 and 7.7 GPa, respectively. The superconductive transition for the wires was attributed to structural reconstruction in the grain boundary areas. For bulk rhomobohedral bismuth superconductivity was not yet found down to 50 mK, while amorphous bismuth becomes superconductive at ~ 6 K.

3.2 Quantum-size effects

In low-dimensional materials the density of states is modified due to spatial confinement. This enables the manipulation of the transport properties of low-dimensional structures. For instance, the confinement of the electron gas in a low-dimensional system causes an oscillation of the electronic transport characteristics as a function of the structure size. Such kind of oscillations were found for bismuth thin films (Duggal & Rup, 1969), (Rogacheva et al., 2003) and very recently also for Bi nanowires by Farhangfar (Farhangfar, 2007) and Cornelius et al. (Cornelius et al., 2008). Also, oscillations with diffreent periodicity and magnitude were reported for rectangular and cylindrical nanowires. On the one hand, the conductivity of rectangular nanowires was measured on an individual wire whose width was reduced gradually by reactive ion etching. On the other hand, single cylindrical nanowires were prepared in a single-pore membrane. The different oscillatory characteristics can originate from the different wire cross-sections or from different surface properties. While the etching process applied to the rectangular nanowires may influence the surface roughness and, thus, the electron scattering at the surface, the cylindrical nanowires were left embedded in the polymer membrane in order to avoid any surface modification due to oxidation or to reactions with the solvent when removing the template. In the case of single cylindrical nanowires, the electrical conductivity oscillates as a function of the wire diameter (Fig. 15). These modulatione have been described by exponential functions $\sigma \sim \exp(-d/d_c)$. The periodicity is extracted from the intersection points of the extrapolated fitting curves (represented by dotted lines) with the x-axis. The first intersection point represents the critical diameter for the semimetal-semiconductor transition amounting to d_c = 40 nm. Fitting this experimentally found d_c value by equation (5) using E_F = 56 meV (Black et al., 2000), m^* = 0.0022 m_e is derived for bulk Bi, in reasonable agreement with the value correspondent to electrons at the L-point. The critical diameters amount to 40, 115, 182, 281, and 358 nm. This progression can be approximated by a $d_{c_n} \sim (n+1/2)d_0$ proportionality with d_0 = 80 nm and n being a natural number including zero similar to the energy levels of a harmonic oscillator.

The exponential behaviour of the oscillations may be explained by the thermal excitation of charge carriers. Only charge carriers close to the Fermi level contribute to the electrical transport. When a subband passes E_F, it is depleted and the charge carriers are transferred to lower states. At RT, they are excited thermally to higher subbands so that they participate in the electrical transport. With increasing band gap, i.e., decreasing wire diameter, the number of thermally excited carriers decreases and, thus, the electrical conductivity drops. As soon as a lower subband approaches E_F, the charge carrier density recovers and, hence, the conductivity increases to about 3000 S/cm being in agreement with the mean resistivity of 440 μΩ cm (σ = 2272 S/cm) reported in (Cornelius et al., 2006). The whole process occurs repeatedly until the lowest subband passed the Fermi level and the material is transferred into a semiconductor.

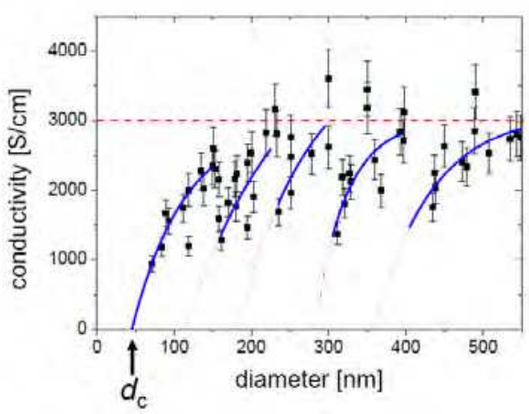

Fig. 15. Specific electrical conductivity of single Bi nanowires as a function of diameter.

4. Infrared optical properties

Infrared spectroscopy was performed on bismuth nanowire arrays embedded in alumina templates, on free-standing wire arrays, and on single nanowires that were placed on a Si wafer. The interpretation of spectroscopic features from arrays is rather complicated: the dielectric properties (in particular, vibration excitations) of an embedding material do not necessarily cancel out by measuring relative spectra and, furthermore, the spectra measured on nanowire arrays can be affected by the electromagnetic coupling of neighbouring needles. In order to separate the contributions of the wires and the alumina template an effective medium theory (EMT) was employed. In order to perform infrared spectroscopy on single bismuth nanowires the ion track-etched polymer membrane was dissolved in DMF and, subsequently, few drops of the solvent containing clean wires were put on a Si substrate. The single wires lying on the wafer were investigated at room temperature by spectroscopic microscopy at the IR beamline of the ANKA synchrotron light source at Forschungszentrum Karlsruhe. Single nanowires were located by means of optical microscopy and, subsequently, selecetd by an aperture with diameter 8 μm in the focal plane of the microsopce. IR transmission spectroscopy was performed at normal incidence of light from 800 to 5500 cm^{-1}. For this purpose, a Fourier transform IR spectrometer (Bruker IFS 66v/S) with a cooled mercury–cadmium–telluride detector was used. Nearby areas without any wires were selected for reference measurements. To obtain the relative IR transmission $T_{rel}(\omega)$ of a single wire, the substrate intensity $I_{ref}(\omega)$ is substracted from the wire signal $I_{wire}(\omega)$ by

$$T_{rel}(\omega) = \frac{I_{wire}}{I_{ref}} \tag{8}$$

and the absorption spectra $A(\omega)$ are calculated by means of equation (9).

$$A(\omega) = 1 - T_{rel}(\omega) \tag{9}$$

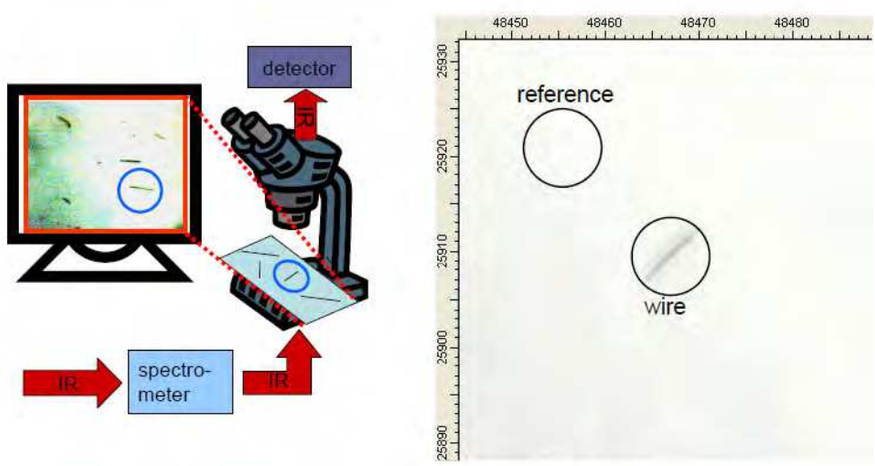

Fig. 16. Schematic of experimental setup. Optical microscopy image of single Bi nanowire of d = 200 nm on a Si wafer. The two circles correspond to the locations where IR spectroscopy has been performed: (1) single wire and (2) reference position.

Experiments on single <110> textured bismuth nanowires with various diameters lying on a Si wafer revealed a pronounced infared absorption (Fig. 17). The absorption onsets are defined by the intersection of the dashed lines (extrapolation of the strongest absorption increase) and the *x*-axis. The absorption edge was found to be blue-shifted with diminishing wire diameter. For instance, it is located at 1100 and 3500 cm^{-1} for wires with diameter of 400 and 30 nm, respectively. This absorption is ascribed to direct transitions in the vicinity of the L-point of the Brillouin zone and the blueshift is assigned to quantum size effects which involve

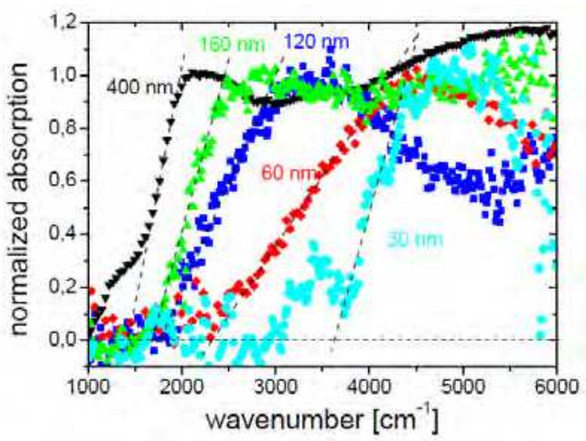

Fig. 17. Normalized infrared absorption spectra of single bismuth nanowires with different diameters.

a subband splitting of the energy bands. Hence, the band edges at the L-point shift away from each other leading to an increase of the forbidden band with decreasing specimen size.
For free-standing <012> textured Bi nanowires with diameter 45 nm a strong absorption at ~ 1050 cm^{-1} was found. In addition to this large peak, smaller absorption signals were observed at ~ 616, ~ 667, ~ 798, and ~ 986 cm^{-1}. These peaks were not seen for the nanowires embedded in alumina. The strong absorption signal at 1050 cm^{-1} was attributed to an indirect transition from the L-point valence band to the T-point valence band while no indication for direct transitions were found as for single wires located on a Si wafer. For bulk Bi this transition is very weakly pronounced due to the necessity of a phonon for changing the momentum of the excited electron while it surpasses all other signals in the case of these nanowires. Due to the spatial confinement in low-dimensional systems electrons may be effectively scattered at the surface and, thus, different points in the Brillouin zone are accessible by the excited charge carriers. Hence, no phnons are needed for those indirect transitions in low-dimensional systems. Note that the connections of different points in the Brillouin zone depend on the crystalline orientation of the system. This additional path for indirect transitions is also the explanation for the different absorption spectra of nanowires possessing different crystalline orientation. The other, smaller peaks in the spectrum are ascribed to intraband excitations which can only be found for low-dimensional structures. Because of quantum-size effects the energy bands split in sublevels.

5. Burn-out current density

Studies of the maximum current density of single bismuth nanowires were carried out. For this purpose, single Bi wires were electrochemically deposited in single-pore ion track-etched polycarbonate mebranes as described in CHAPTER 2. After electrical contacting (Fig. 11(c)), I-V characteristics were measured, ramping up the current in 50 μA steps until failure occurred. Figure 18(a) displays the *V-I* curve of a single bismuth nanowire with diameter 230 nm (deposition conditions: T = 50 °C, U = −25 mV). The wire exhibits an Ohmic behavior (linear *V-I* curve) for currents up to 800 μA. Shortly before breakage, the *V-I* curve deviates from the linear behavior. The wire fails at I = 960 μA, i.e., the wire is able to carry a current density of j_{max} = 2.31 x 10^6 A/cm^2. This j_{max} is more than two orders of magnitude higher than in bulk metals such as Cu and Au and three to four orders of magnitude higher than expected for bulk bismuth.
In Fig. 18(b), the burnout current density is plotted as a function of the inverse wire diameter for several single bismuth nanowires, evidencing a direct proportionality between I_{max} and d^{-1}. Our experiments reveal that wires with diameter of 1 μm may carry j_{max} ~ 5 x 10^5 A/cm^2 and that the maximum current density increases with decreasing wire diameter. For metal thin films grown on substrates, it was found that j_{max} amounts to 10^4 – 10^6 A/cm^2, i.e., these films can carry one to two orders of magnitude higher current densities than their bulk counterparts. The increase in j_{max} was attributed to the fact that the film dissipates the heat to the substrate. Similarly, nanowires embedded in a template may dissipate heat to the surrounding polymer. The heat dissipation will be more efficient for thinner nanowires that possess a higher surface-to-volume ratio. The results in Fig. 18(b) evidence that wires created at higher temperature and smaller overpotential (blue empty circles) can systematically carry higher current densities than wires created at higher voltages and lower temperatures (black filled squares). This is explained either by the fact that these wires contain less grain boundaries where mostly atom diffusion takes place, or that a smaller number of grain boundaries involves a smaller specific electrical resistivity and, hence, less Joule heat is generated.

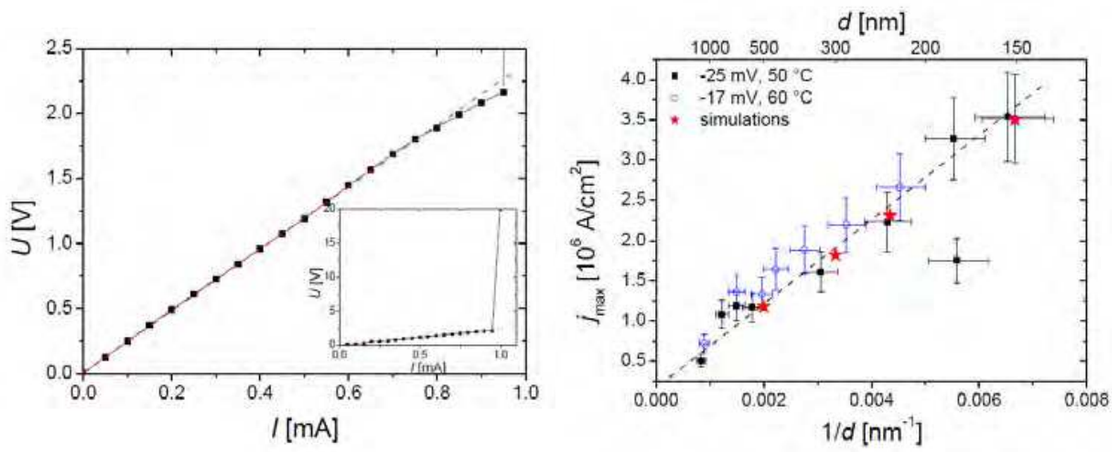

Fig. 18. (a) *U-I* characteristic of a single bismuth nanowire embedded in the PC membrane and contacted between two macroscopic contacts displaying the burn-out current density. The inset displays a zoom in at the maximal current density. (b) Maximal current density vs d^{-1} for single nanowires created under two different deposition conditions.

The failure of the nanowires can be attributed to either Joule heating or electromigration, or a combination of both. The temperature of a wire with diameter of 230 nm embedded in a template with a model diameter of 1 mm and thickness 30 μm was simulated by using the commercial software COMSOL MULTIPHYSICS. For computations, the thermal conductivities of the polymer template and the bismuth wires were 0.2 and 4 W m^{-1} K^{-1} (as known from Bi thin films (Völklein & Kessler, 1986)), respectively. We assumed a reduced thermal conductivity of the wires compared to bulk bismuth (κ_{bulk} = 7.87 W m^{-1} K^{-1}) due to finite-size effects. The thermal conductivity of the metal coatings on both sides of the template was 400 W m^{-1} K^{-1}. As mentioned above, the current density j_{max} of the nanowire with 230 nm diameter was 2.31 x 10^6 A/cm^2. Since the generated Joule heat is dissipated to the ambient by convection and radiation at the metallic surfaces, Neumann boundary conditions have been chosen at these surfaces with heat transfer coefficient α = 6.2 W/(m^2 K) for convection and emissivity ε = 0.05 for thermal radiation heat transfer according to the Stefan–Boltzmann law. The calculated temperatures along the nanowire axis and normal to the wire (through its center) along a radial line through the template are presented in Figs. 19(a) and (b), respectively. The temperature of the wire contacts with the metal coatings remains at room temperature while the central 10 μm of the wire are heated to 542 K. Moreover, the temperature decreases to room temperature radially around the wire within 30 μm in the template material. The computed maximal temperature of the wire reaches almost the melting temperature of bulk bismuth (T_m = 544 K) indicating that the wire fails due to Joule heating. The asterisks in Figure 18(b) represent the calculated maximum current densities assuming wire failure due to Joule heating. The computed j_{max} values are in excellent agreement with the exerperimentally determined current denisties.

6. Conclusion

In conclusion, bismuth is, due to its extraordinary electronic properties, namely a long mean free path of 100 nm, a large Fermi wavelength of 40 nm, and a very small electron effective mass (0.001 – 0.26 m_e), an excellent material to study the influence of finite-size and quantum-size effects on the transport properties of nanostructures. For the study of these

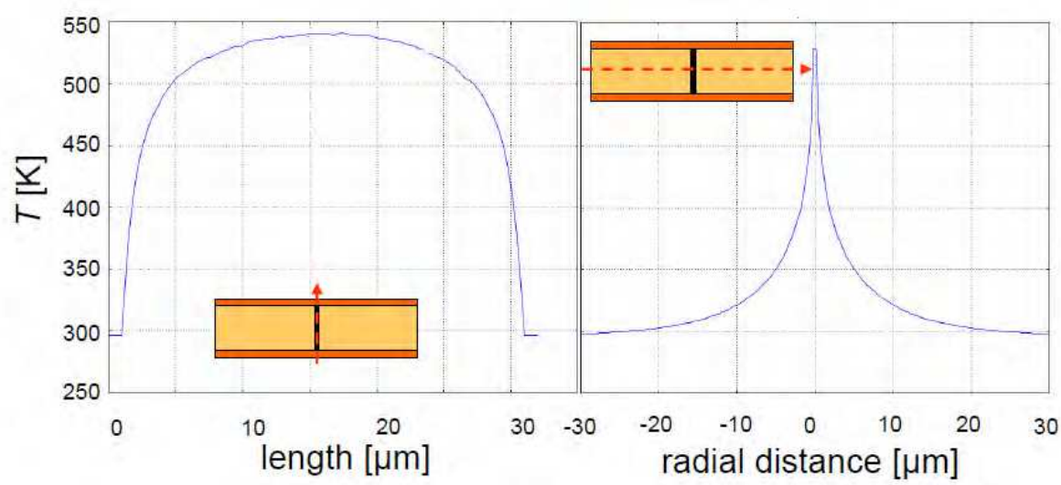

Fig. 19. Simulated temperature profiles for a Bi nanowire of diameter 230 nm embedded in the template along the wire axis and across the wire center. The insets indicate the scanning directions.

effects, nanowire arrays as well as individual nanowires have been created by numerous techniques including a solvothermal process, electron beam lithography, the Taylor process, and the template method. Depending on the fabrication method, polycrystalline and single-crystalline wires with different preferred orientations have been grown. Measurements of the electrical conductance of both nanowire arrays and individual nanowires have evidenced a very strong influence of the wire crystallinity on the electrical resistivity value. In particular, the resistivity increases with respect to bulk with decreasing grain size, as predicted by the Mayadas-Shatzkes model. Moreover, resistance measurements as a function of temperature revealed a strong reduction of the charge carrier mobility originating from additional electron scattering processes at grain boundaries. This reduction of the mobility leads to a non-monotonic resistance vs temperature behaviour for wires consisting of large grains and a monotonic increasing resistance with decreasing temperature for fine-grained wires. In addition, studies of the electrical resistivity on individual wires as a function of the wire diameter revealed an oscillatory behaviour that has been attributed to quantum-size effects causing a splitting of the energy bands in subbands and, thus, to a modulation of the charge carrier density at the Fermi level. These novel findings are further supported by recent infrared spectroscopy experiments. For <012> textured wire arrays infrared absorptions were reported stemming from intraband excitations, i.e., excitations of the electrons from one subband to another. In addition, for single <110> textured wires an infrared absorption was found whose edge shifts to higher energies with decreasing wire diameter due to the shift of the band edges away from each and, hence, increasing the direct band gap in the vicinity of the L-point. The fact that different absorption spectra were found for differently textured nanowires was attributed to the possibility that electrons can be effectively scattered at the surface of spatially confined materials and, thus, making different points of the Brillouin zone accessible. Last but not least, studies on single bismuth nanowires embedded in the polymer template evidenced burn-out current densities 3 to 4 orders of magnitude larger than for bulk bismuth. In addition, the thinner the wire diameter, the larger the maximal current supported by the single nanowire. This effect is attributed to a more efficient heat dissipation from the wire to the surrounding polymer, for nanowires displaying higher surface-to-volume ratio.

7. References

Apel, P.Yu.; Spohr, R.; Trautmann, C.; Vutsadakis, V. (1999). Track structure in polyethylene terephthalate irradiated by heavy ions: Let dependence of track diameter. *Radiat. Meas.* 31 (1999) 51 – 56.

Barati, M.; Sadeghi, E. (2001). Study of ordinary size effect in the electrical conductivity of Bi nanowires. *Nanotechnology* 12 (2001) 277 – 280.

Bate, R.T.; Einspruch, N.G. (1967). Galvanomagnetic studies of Sn-doped Bi. I. Positive Fermi energies. *Phys. Rev.* 153 (1967) 796 – 799.

Black, M.R.; Padi, M.; Cronin, S.B.; Lin, Y.-M.; Rabin, O.; McClure, T.; Dresselhaus, G.; Hagelstein, P.L.; Dresselhaus, M.S. (2000). Intersubband transitions in bismuth nanowires. *Appl. Phys. Lett.* 77 (2000) 4142 – 4144.

Black, M.R.; Lin, Y.-M.; Cronin, S.B.; Rabin, O.; Dresselhaus, M.S. (2002). Infrared absorption in bismuth nanowires resulting from quantum confinement. *Phys. Rev. B* 65 (2002) 195417.

Black, M.R.; Hagelstein, P.L.; Cronin, S.B.; Lin, Y.M.; Dresselhaus, M.S. (2003). Optical absorption from indirect transition in bismuth nanowires. *Phys. Rev. B* 68 (2003) 235417.

Black, J.R. (1969). Electromigration – A brief survey of recent results. *IEEE Trans. Electron. Devices ED*-16 (1969) 338 – 347.

Chiu, P.; Shih, I. (2004). A study of the size effect on the temperature-dependent resistivity of bismuth nanowires with rectangular cross-section. *Nanotechnology* 15 (2004) 1489 – 1492.

Chtanko, N.; Toimil Molares, M.E.; Cornelius, Th.; Dobrev, D.; Neumann, R. (2004). Etched single-ion-track templates for single nanowire synthesis. *J. Phys. Chem. B* 108 (2004) 9950 – 9954.

Cornelius, T.W.; Apel, P.Yu.; Schiedt, B.; Trautmann, C.; Toimil Molares, M.E.; Karim, S.; Neumann, R. (2007). Investigation of nanopore evolution in ion track-etched polycarbonate membranes. *Nucl. Instr. Meth. B* 265 (2007) 553 – 557.

Cornelius, T.W.; Brötz, J.; Chtanko, N.; Dobrev, D.; Miehe, G.; Neumann, R.; Toimil Molares, M.E. (2005). Controlled fabrication of poly- and single-crystalline bismuth nanowires. *Nanotechnology* 16 (2005) S246 – S249.

Cornelius, T.W.; Toimil-Molares, M.E.; Karim, S.; Neumann, R. (2008). Oscillations of electrical conductivity in single bismuth nanowires. *Phys. Rev. B* 77 (2008) 125425.

Cornelius, T.W.; Toimil-Molares, M.E.; Lovrincic, R.; Karim, S.; Neumann, R.; Pucci, A.; Fahsold, G. (2006). Quantum size effects manifest in infrared properties of single bismuth nanowires. *Appl. Phys. Lett.* 88 (2006) 103114.

Cornelius, T.W.; Toimil-Molares, M.E.; Neumann, R.; Karim, S. (2006). Finite-size effects in the electrical transport properties of single bismuth nanowires. *J. Appl. Phys.* 100 (2006) 114307.

Cronin, S.B.; Lin, Y.-M.; Rabin, O.; Black, M.R.; Ying, J.Y.; Dresselhaus, M.S.; Gai, P.L.; Minet, J.-P.; Issi, J.-P. (2002). Making electrical contacts to nanowires with a thick oxide coating. *Nanotechnology*, 13 (2002) 653 – 658.

Dai, H.; Wong, E.W.; Lieber, C.M. (1996). Probing electrical transport in nanomaterials: conductivity of individualcarbon nanotubes. *Science* 272 (1996) 523 – 526.

Dingle, R.B. (1950). The elctrical conductivity of thin wires. *Proc. Roy. Soc. A* 201 (1950) 545 – 560.

Duggal, V.P.; Rup, R. (1969). Thickness-dependent oscillatory behavior of resistivity and Hall coefficient in thin single-crystal bismuth films. *J. Appl. Phys.* 40 (1969) 492 – 495.

Farhangfar, S. (2006). Quantum size effects in a one-dimensional semimetal. *Phys. Rev. B* 74 (2006) 205318.

Farhangfar, S. (2007). Quantum size effects in solitary wires of bismuth. *Phys. Rev. B* 76 (2007) 205437.

Fuchs, K (1938). The conductivity of thin metallic films according to the electron theory of metals. *Proc. Cambridge Philos. Soc.* 34 (1938) 100.

Gao, Y.; Niu, H.; Zeng, C.; Chen, Q. (2003). Preparation and characterization of single-crystalline bismuth nanowires by a low-temperature solvothermal process. *Chem. Phys. Lett.* 367 (2003) 141 – 144.

Gallo, C.F.; Chandrasekhar, B.S.; Sutter, P.H. (1962). Transport properties of bismuth single crystals. *J. Appl. Phys.* 34 (1962) 144 – 152.

Glocker, D.A.; Skove, M.J. (1977). Field effect and magnetoresistance in small bismuth wires. *Phys. Rev. B* 15 (1977) 608 – 616.

Garcia, N.; Kao, Y.H.; Strongin, M. (1972). Galvanomagnetic studies of bismuth films in the quantum-size-effect region. *Phys. Rev. B* 5 (1972) 2029 – 2039.

Heremans, J.; Thrush, C.M.; Lin, Y.-M.; Cronin, S.; Zhang, Z.; Dresselhaus, M.S.; Mansfield, J.F. (2000). Bismuth nanowire arrays: Synthesis and galvanomagneitic properties. *Phys. Rev. B* 61 (2000) 2921 – 2930.

Heremans, J.; Thrush, C.M.; Zhang, Z.; Sun, X.; Dresselhaus, M.S. (1998). Magnetoresistance of bismuth nanowire arrays. A possible transition from one-dimensional to three-dimensional localization. *Phys. Rev. B* 58 (1998) R10091.

Ho, P.S.; Kwok, T. (1989). Electromigration in metals. *Rep. Prog. Phys.* 52 (1989) 301 – 348.

Hofmann, P. (2005). *The surfaces of bismuth: Structural and electronic properties*. University of Aarhus (2005)

Huber, T.E.; Celestine, K.; Graf, M.J. (2003). Magntoquantum oscillations and confinement effects in arrays of 270-nm-diameter bismuth nanowires. *Phys. Rev. B* 67 (2003) 245317.

Isaacson, R.T.; Williams, G.A. (1969). Alfvén-wave propagation in solid-state plasmas. III. Quantum oscillations of the Fermi surface of bismuth. *Phys. Rev.* 185 (1969) 682 – 688.

Kaiser, Ch.; Weiss, G.; Cornelius, T.W.; Toimil Molares, M.E.; Neumann, R. (2009). Low temperature magnetoresistance measurements on bismuth nanowire arrays. *J. Phys.: Condens. Matter* 21 (2009) 205301.

Karim, S.; Toimil-Molares, M.E.; Maurer, F.; Miehe, G.; Ensinger, W.; Liu, J.; Cornelius, T.W.; Neumann, R. (2006). Synthesis of gold nanowires with controlled crystallographic characteristics. *Appl. Phys. A* 84 (2006) 403 – 407.

Lax, B.; Mavroides, J.G.; Zeiger, H.J.; Keyes, R.J. (1960). Infrared magneotreflection in bismuth. I. High fields. *Phys. Rev. Lett.* 5 (1960) 241 – 243.

Li, L.; Zhang, Y.; Li, G.; Wang, X.; Zhang, L. (2005). Synthetic control of large-area, ordered bismuth nanowire arrays. *Mater. Lett.* 59 (2005) 1223 – 1226.

Lin, Y.-M.; Cronin, S.B.; Ying, J.Y.; Dresselhaus, M.S.; Heremans, J.P. (2000). Transport properties of Bi nanowire arrays. *Appl. Phys. Lett.* 76 (2000) 3944 – 3946.

Lin, Y.-M.; Sun, X.; Dresselhaus, M.S. (2000). Theoretical investigation of thermoelectric transport properties of cylindrical Bi nanowires. *Phys. Rev. B* 62 (2000) 4610 – 4623.

Liu, K.; Chien, C.L.; Searson, P.C.; Yu-Shang, K. (1998). Structural and magneto-transport properties of electrodeposited bismuth nanowires. *Appl. Phys. Lett.* 73 (1998) 1436 – 1438.

MacDonald, D.K.C.; Sarginson, K. (1950). Size effect variation of the electrical conductivity of metals. *Proc. Roy Soc. A* 203 (1950) 223 – 240.

Martin, C.R. (1994). Nanomaterials: A membrane-based synthetic approach. *Science* 266 (1994) 1961 – 1966.

Masuda H.; Nishio, K. (2006). Synthesis and Applications of Highly Ordered Anodic Porous Alumina. In: *Self organized nanoscale materials*, 296 – 312, Springer New York, ISBN 978-0-387-27975-6

Mayadas, A.F.; Shatzkes, M (1970). Electrical-resistivity model for polycrystalline films: the case of arbitrary reflection at external surfaces. *Phys. Rev. B* 1 (1970) 1382 – 1389.

Nikolaeva, A.; Gitsu, D.; Konopko, L.; Graf, M.J.; Huber, T.E. (2009). Quantum interference of surface states in bismuth nanowires probed by the Aharonov-Bohm oscillation of the magnetoresistance. *Phys. Rev. B* 77 (2008) 075332.

Omaggio, J.P.; Meyer, J.R.; Hoffmann, C.A.; DiVenere, A.; Yi, X.J.; Hou, C.L.; Wang, H.C.; Ketterson, J.B.; Wong, G.K.; Heremans, J.P. (1993). Magneto-optical determination of the T-point energy gap in bismuth. *Phys. Rev. B* 48 (1993) 11439 – 11442.

Parrott, J.E. (1965). A new theory of the size effect in electrical conduction. *Proc. Phys. Soc.* 85 (1965) 1143 – 155.

Rogacheva, E.I.; Grigorov, S.N.; Nashchekina, O.N.; Lyubchenko, S.; Dresselhaus, M.S. (2003). Quantum-size effects in *n*-type bismuth thin films. *Appl. Phys. Lett.* 82 (2003) 2628 – 2630.

Sandormirskiĭ, V.B. (1967). Quantum size effects in a semimetal film. *Sov. Phys. JETP* 25 (1967) 101

Schönenberger, C.; van der Zande, B.M.I.; Fokkink, L.G.J.; Henny, M.; Schmid, C.; Krüger, M.; Bachtold, A.; Huber, R.; Birk, H.; Staufer, U. (1997). Template synthesis of nanowires in porous polycarbonate membranes: Electrrochemistry and morphology. *J. Phys. Chem. B* 101 (1997) 5497 – 5505.

Siwy, Z.; Apel, P.; Baur, D.; Dobrev, D.; Korchev, Y.E.; Neumann, R.; Spohr, R.; Trautmann, C.; Voss, K.O. (2003). Preparation of synthetic nanopores with transport properties analogous to biological channels. *Surf. Sci.* 532-535 (2003) 1061 – 1066.

Tian, M.; Wang, J.; Kumar, N.; Han, T.; Kobayashi, Y.; Liu, Y.; Mallouk, T.E.; Chan, M.H.W. (2006). Observation of superconductivity in granular Bi nanowires fabrictaed by electrodeposition. *Nano Lett.* 6 (2006) 2773 – 2780.

Toimil Molares, M.E.; Buschmann, V.; Dobrev, D.; Neumann, R.; Scholz, R.; Schuchert, I.U.; Vetter, J. (2001). Single-crystalline copper nanowires produced by electrochemical deposition in polymeric ion track membranes. *Adv. Mater.* 13 (2001) 62 – 65.

Toimil Molares, M.E.; Chtanko, N.; Cornelius, T.W.; Dobrev, D.; Enculescu, I.; Blick, R.H.; Neumann, R. (2004). Fabrication and contacting of single Bi nanowires. *Nanotechnology* 15 (2004) S201 – S207.

Völklein, F.; Kessler, E. (1986). Analysis of the lattice thermal conductivity of thin films by means of a modified Mayadas-Shatzkes model. *Thin Solid Films* 142 (1986) 169 – 181.

Wang, X.F.; Zhang, L.D.; Zhang, J.; Shi, H.Z.; Peng, X.S.; Zheng, M.J.; Fang, J.; Chen, J.L.; Gao, B.J. (2001). Ordered single-crystalline Bi nanowire arrays embedded in nanochannels of anodic alumina membranes. *J. Phys. D: Appl. Phys.* 34 (2001) 418 – 421.

Yin, A.J.; Li, J.; Jian, W.; Bennett, A.J.; Xu, J.M. (2001). Fabrication of highly ordered metallic nanowire arrays by electrodeposition. *Appl. Phys. Lett.* 79 (2001) 1039 – 1041.

Zhang, Z.; Ying, J.Y.; Dresselhaus, M.S. (1998). Bismtuh quantum-wire arrays fabricated by a vacuum melting and pressure injection process. *J. Mater. Res.* 13 (1998) 1745 – 1748.

Zhang, Z.; Sun, X.; Dresselhaus, M. S.; Ying, J. Y.; Heremans, J. (2000). Electronic transport properties of single-crystal bismuth nanowire arrays. *Phys. Rev. B* 61 (2000) 4850 – 4861.

Nanowires

Edited by Paola Prete

ISBN 978-953-7619-79-4
Hard cover, 414 pages
Publisher InTech
Published online 01, February, 2010
Published in print edition February, 2010

This volume is intended to orient the reader in the fast developing field of semiconductor nanowires, by providing a series of self-contained monographs focusing on various nanowire-related topics. Each monograph serves as a short review of previous results in the literature and description of methods used in the field, as well as a summary of the authors recent achievements on the subject. Each report provides a brief sketch of the historical background behind, the physical and/or chemical principles underlying a specific nanowire fabrication/characterization technique, or the experimental/theoretical methods used to study a given nanowire property or device. Despite the diverse topics covered, the volume does appear as a unit. The writing is generally clear and precise, and the numerous illustrations provide an easier understanding of the phenomena described. The volume contains 20 Chapters covering altogether many (although not all) semiconductors of technological interest, starting with the IV-IV group compounds (SiC and SiGe), carrying on with the binary and ternary compounds of the III-V (GaAs, AlGaAs, GaSb, InAs, GaP, InP, and GaN) and II-VI (HgTe, HgCdTe) families, the metal oxides (CuO, ZnO, ZnCoO, tungsten oxide, and PbTiO3), and finishing with Bi (a semimetal).

How to reference
In order to correctly reference this scholarly work, feel free to copy and paste the following:

Thomas W. Cornelius and M. Eugenia Toimil-Molares (2010). Finite- and Quantum-Size Effects of Bismuth Nanowires, Nanowires, Paola Prete (Ed.), ISBN: 978-953-7619-79-4, InTech, Available from: http://www.intechopen.com/books/nanowires/finite-and-quantum-size-effects-of-bismuth-nanowires

INTECH
open science | open minds

InTech Europe
University Campus STeP Ri
Slavka Krautzeka 83/A
51000 Rijeka, Croatia
Phone: +385 (51) 770 447
Fax: +385 (51) 686 166
www.intechopen.com

InTech China
Unit 405, Office Block, Hotel Equatorial Shanghai
No.65, Yan An Road (West), Shanghai, 200040, China
中国上海市延安西路65号上海国际贵都大饭店办公楼405单元
Phone: +86-21-62489820
Fax: +86-21-62489821

© 2010 The Author(s). Licensee IntechOpen. This chapter is distributed under the terms of the Creative Commons Attribution-NonCommercial-ShareAlike-3.0 License, which permits use, distribution and reproduction for non-commercial purposes, provided the original is properly cited and derivative works building on this content are distributed under the same license.

IntechOpen

IntechOpen